

# On the Estimation of Bivariate Return Curves for Extreme Values

C. J. R. Murphy-Barltrop<sup>1\*</sup>, J. L. Wadsworth<sup>2</sup> and E. F. Eastoe<sup>2</sup>

<sup>1</sup>STOR-i Centre for Doctoral Training, Lancaster University LA1 4YR, United Kingdom

<sup>2</sup>Department of Mathematics and Statistics, Lancaster University LA1 4YR, United Kingdom

\*Correspondence to: c.barltrop@lancaster.ac.uk

May 23, 2022

## Abstract

In the multivariate setting, defining extremal risk measures is important in many contexts, such as finance, environmental planning and structural engineering. In this paper, we review the literature on extremal bivariate return curves, a risk measure that is the natural bivariate extension to a return level, and propose new estimation methods based on multivariate extreme value models that can account for both asymptotic dependence and asymptotic independence. We identify gaps in the existing literature and propose novel tools for testing and validating return curves and comparing estimates from a range of multivariate models. These tools are then used to compare a selection of models through simulation and case studies. We conclude with a discussion and list some of the challenges.

*Keywords:* Risk Measure, Extremes, Dependence Modelling

# 1 Introduction

## 1.1 Univariate Extremal Risk Measures

Statistical analysis of extreme values is important in a wide range of contexts, from hydrology to insurance. The two most common approaches to modelling the extreme behaviour (or tail) of a single variable are block maxima and peaks over threshold (Coles, 2001). For the former approach, the generalised extreme value (GEV) distribution is used to model the stochastic behaviour of maxima from large blocks of observations. If a random variable  $M$  has a GEV distribution function, we write  $M \sim \text{GEV}(\mu, \sigma, \xi)$ , with the cumulative distribution function (cdf) given by  $\Pr(M \leq x) = \exp \left\{ - \left[ 1 + \xi \left( \frac{x-\mu}{\sigma} \right) \right]^{-1/\xi} \right\}$  for  $\xi \neq 0$  and  $\Pr(M \leq x) = \exp \left\{ - \exp \left( -\frac{x-\mu}{\sigma} \right) \right\}$  for  $\xi = 0$ . We refer to  $\mu, \sigma$  and  $\xi$  as location, scale and shape parameters, respectively. The shape parameter  $\xi$  dictates the heaviness of the tail, with  $\xi < 0$ ,  $\xi = 0$  and  $\xi > 0$  corresponding to bounded, exponential and heavy tails, respectively. The peaks over threshold approach requires a model for the stochastic behaviour of all sufficiently large observations. One of two equivalent methods can be used: either a non-homogeneous Poisson process (PP) model or a Poisson-generalised Pareto (GP) model. Both univariate approaches are closely linked and for the GEV and PP models, the corresponding parameter vectors are identical.

Often, models from univariate extreme value theory are used to estimate risk measures for events associated with small probabilities; these summary statistics could help mitigate against rare events, such as floods, storms, or wildfires. One such measure is known as a return level. Given a real variable  $X$ , representing a measurement taken at regular time intervals, and probability  $p$ , the  $p$ -probability return level is the value  $x_p$  that satisfies the equation  $\Pr(X > x_p) = p$ . For small  $p$ ,  $x_p$  represents a high quantile, which can be estimated using the GEV or GP model. We define the return period of  $x_p$  to be the value  $1/p$ ; we expect the variable  $X$  to exceed  $x_p$  once, on average, during each return period.

For example, if  $X$  represents yearly maxima of some phenomenon, then  $x_{0.01}$  is the value we would expect  $X$  to exceed, on average, once every 100 years. The relationship between return levels and periods can be illustrated using a return level plot. Examples of three such plots for the GEV model are shown in Figure 1. One can clearly observe the relationship between the shape parameter and the tail behaviour.

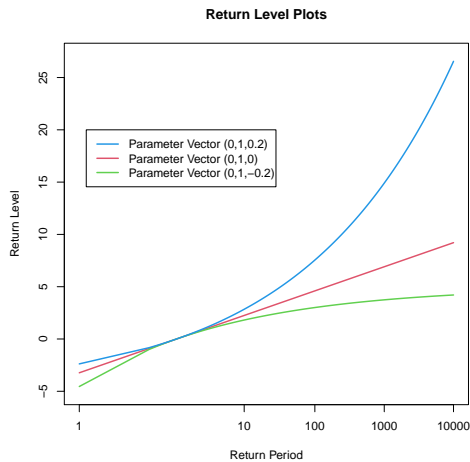


Figure 1: Return level plots for the GEV model with different parameter vectors.

Return levels are widely used and provide a simple way to understand risk. However, many potentially impactful events arise due to the effect of more than one variable (Mattei et al., 2001). For this reason, it is desirable to have equivalent risk measure in the multivariate case, but thus far relatively little consideration has been given to this problem in the multivariate setting. This is in part due to the lack of natural ordering for multivariate vectors, which means there is no longer a single definition of extreme events. Moreover, uncertainty quantification and diagnostic tools for multivariate measures have seldom been considered. In this article, we review existing methods and propose new estimation techniques, restricting attention to the bivariate setting for the sake of simplicity. However, much of the theory discussed can be easily extended to the general multivariate setting.

## 1.2 Return Curves

Given a bivariate random vector  $(X, Y)$  corresponding to measurements records at regular time points, a variety of potential risk measures exist (Serinaldi, 2015). We restrict our attention to one particular measure which directly extends the return level concept to the multivariate setting. Consider the joint survival function of  $(X, Y)$  at a given probability  $p$ , i.e.  $\Pr(X > x, Y > y) = p$ . We aim to find combinations of values  $(x, y) \in \mathbb{R}^2$  such that this equation is satisfied. These combinations define a curve in the plane, hence we define a  $p$ -probability return curve to be the set  $R(p) := \{(x, y) \in \mathbb{R}^2 : \Pr(X > x, Y > y) = p\}$ . Again, we consider values of  $p$  close to zero, corresponding to rare joint exceedance events. Within the literature, this set has a variety of labels, including isolines (Cooley et al., 2019), environmental contours (Ross et al., 2020) and joint probability curves (Gouldby et al., 2017). In an analogue to return levels, we define the return period to be  $1/p$ , since given any point  $(x, y) \in R(p)$ , we would expect to observe the event  $\{X > x, Y > y\}$  once, on average, each return period.

Since the return curve defines a set of points in  $\mathbb{R}^2$  rather than a single value, the two dimensional return level plot does not naturally extend to this setting. Instead, we can consider return periods and plot the corresponding curves individually or simultaneously; examples of both are given in Figure 2 for a standard bivariate normal data set with correlation coefficient  $\rho = 0.5$ .

Return curves are arguably the most intuitive multivariate extension to return levels since they are also defined in terms of the survivor function. They are widely used in practice to derive extremal environmental conditions for the design and analysis of various structures, including ocean structures, such as oil rigs (Jonathan et al., 2014), freight ships (Vanem et al., 2020) and wind turbines (Manuel et al., 2018; Velarde et al., 2019), and coastal structures, such as railway lines (Environmental Agency, 2005; Gouldby et al.,

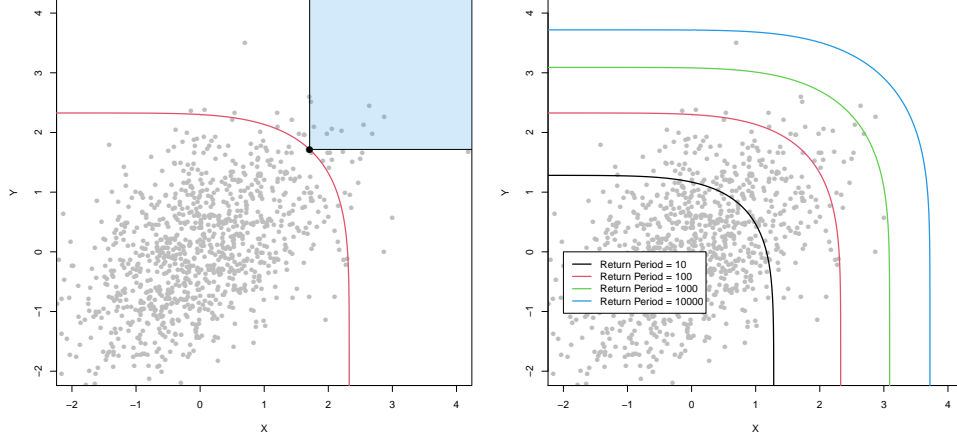


Figure 2: Standard bivariate normal data with  $\rho = 0.5$  and  $n = 1000$ . Left: return curve  $R(p)$  (red) for return period of 100 ( $p = 1/100$ ). Right: return curves for return periods in the set  $\{10, 100, 1000, 10000\}$ . The probability of observing a point in the blue shaded region is equal to  $p$ ; this probability remains constant for all equivalent shaded regions at any point on the curve.

2017), wave energy converters (Eckert-Gallup and Martin, 2016) and nuclear installations (Simpson and Wadsworth, 2017; Office for Nuclear Regulation, 2018). Care must therefore be taken to ensure estimated curves accurately represent the risks present, along with the uncertainty that arises within the analysis.

### 1.3 Practical considerations for return curve estimation

To estimate return curves in practice, we must first estimate the joint survival function of an observed bivariate process for a fixed probability  $p$ . Since we restrict attention to probabilities close to zero, we require an estimation method that can accurately capture the joint tail behaviour of the process and provide realistic extrapolation to estimate return curves for  $p$  outside of the observation period. For this reason, we restrict attention to models within the realm of multivariate extreme value theory. Unlike in the univariate setting, a wide variety of multivariate approaches exist, with the suitability of a given method depending on underlying features of the random vector and many approaches

limited by the forms of extremal dependence they are able to capture (see Section 2).

We must also consider methods for evaluating the uncertainty associated with return curve estimates. This is a more complex problem in the multivariate setting since there is more than one dimension in which the risk measure can vary. Little attention has been given to this particular problem within the extremes literature, motivating the development of a novel approach for defining return curve uncertainty. Given a data set for which a curve has been estimated at probability  $p$ , it is also essential to evaluate goodness of fit via a diagnostic tool to ensure accuracy.

This article is structured as follows. Section 2 provides a brief background on bivariate extreme value theory. In Section 3, we introduce various properties of return curves, explore existing approaches for curve estimation within the extremes literature and present two novel approaches. Section 4 introduces new tools for evaluating the uncertainty and goodness of fit for return curve estimates. Section 5 presents a simulation study to evaluate the performance of these tools and address the issue of model choice. In Section 6, we apply our methodology to data sets of air pollutants and wave data. We conclude in Section 7.

## 2 Bivariate Extreme Value Theory

Early modelling approaches for bivariate extremes rely on limiting results for componentwise maxima given in de Haan and Resnick (1977). Let  $(X_1, Y_1), (X_2, Y_2), \dots, (X_n, Y_n)$  be independent and identically distributed (i.i.d.) random vectors with marginal standard Fréchet, or  $\text{GEV}(1, 1, 1)$ , distributions. If the distribution of  $M_n = (\max_i(X_i), \max_i(Y_i))/n$  converges as  $n \rightarrow \infty$  to a non-degenerate cumulative distribution function (cdf)  $G$ , then we have that  $G(x, y) = \exp(-V(x, y))$ , where  $V$  is called the exponent function (Beirlant et al., 2004). This function is given by  $V(x, y) = 2 \int_0^1 \max(x/w, y/(1-w))H(dw)$ , where  $H$  denotes the spectral measure satisfying the ‘mean’ constraints  $\int_0^1 wH(dw) =$

$\int_0^1 (1-w)H(dw) = 1/2$ . A cdf  $G$  which satisfies these properties is known as a bivariate extreme value (BEV) distribution.

Unlike for the univariate block maxima approach, BEV distributions cannot be described in a closed parametric form and are instead characterised by any spectral measure satisfying the mean constraints. A variety of approaches exist for modelling bivariate extreme observations using a BEV model. These include defining parametric submodels for the exponent (Coles and Tawn, 1991) or spectral measures (Boldi and Davison, 2007), as well as non-parametric techniques (Einmahl and Segers, 2009). In all approaches, the margins and dependence structure are modelled separately in a similar manner to copula-based modelling. Prior to inference, bivariate observations are therefore first transformed to common margins using the probability integral transform (PIT). This is justified by Sklar's theorem (Sklar, 1959), which states that the dependence structure for a bivariate vector remains constant regardless of the marginal distributions.

In practice, the modelling of component-wise maxima is not particularly useful due to both the limited amount of information available and the fact the values  $(\max_i(X_i), \max_i(Y_i))$  are unlikely to correspond to concurrent values of  $X$  and  $Y$ . Consequently, this has led to the development of alternative, threshold-based approaches motivated by the BEV distribution. These include point-process approaches (Coles and Tawn, 1991) and multivariate generalised Pareto distributions (Rootzén and Tajvidi, 2006) in analogy to univariate extreme value theory.

In many practical applications however, BEV distributions are limited due to the forms of an extremal dependence they are able to capture. Given a random vector  $(X, Y)$  with marginal cdfs  $F_X, F_Y$ , we define the coefficient  $\chi := \lim_{u \rightarrow 1} \chi(u) \in [0, 1]$ , where  $\chi(u) = \Pr(F_Y(Y) > u \mid F_X(X) > u)$ . While  $\chi$  is a limiting measure, the behaviour of  $\chi(u)$  for large  $u$  provides a measure of the strength of dependence within the join tails of  $(X, Y)$ . The cases  $\chi = 0$  and  $\chi > 0$  correspond to asymptotic independence (AI) and asymptotic

dependence (AD), respectively. A larger  $\chi$  corresponds to stronger positive dependence in the joint tail.

Due to the constraints imposed on the exponent and spectral measures, BEV distributions are only able to capture the regimes of AD and complete independence (a special case of AI). This represents a deficiency within this modelling approach, thereby limiting its use in practice. Moreover, assuming the incorrect form of extremal dependence will lead to unsuitable extrapolation in the joint upper tail (Ledford and Tawn, 1997). In practice, unless there is strong prior knowledge in favour of either AD or AI, it is desirable to use models which have sufficient flexibility to allow the data to directly inform the class of extremal dependence structure.

The first such approach was proposed in Ledford and Tawn (1996). Given  $(X, Y)$  with standard Fréchet or Pareto margins, this model assumes the joint tail representation

$$\Pr(X > t, Y > t) = \Pr(\min(X, Y) > t) = L(t)t^{-1/\eta} \text{ as } t \rightarrow \infty,$$

where  $L$  is a slowly varying function at infinity, i.e.  $\lim_{t \rightarrow \infty} (ct)/L(t) = 1$  for  $c > 0$ , and  $\eta \in (0, 1]$ . The parameter  $\eta$  is termed the coefficient of tail dependence, with  $\eta = 1$  and  $\lim_{t \rightarrow \infty} L(t) > 0$  corresponding to AD and  $\eta < 1$ , or  $\eta = 1$  and  $\lim_{t \rightarrow \infty} L(t) = 0$ , corresponding to AI. Defining the variable  $T := \min(X, Y)$ , estimation of  $\eta$  can be performed through the univariate modelling of  $T$ . By the definition of slowly varying functions, it follows that  $\Pr(T > rt \mid T > t) = \frac{L(rt)}{L(t)}r^{-1/\eta} \rightarrow r^{-1/\eta}$  as  $t \rightarrow \infty$  for any  $r > 0$ , allowing the coefficient  $\eta$  to be estimated using the Hill estimator (Hill, 1975). Several extensions to this approach exist, including Ledford and Tawn (1997) and Ramos and Ledford (2009), which allow for bivariate modelling without the need to pre-specify whether data are AD or AI. However, these techniques are applicable only within regions where both variables are large. As a result, these methods are not appropriate for the



estimation of return curves; see Section 3.3 for further details (Cooley et al., 2019).

Wadsworth and Tawn (2013) provide an alternative representation for bivariate tail probabilities using a more general extension of the framework given in Ledford and Tawn (1996). Given  $(X, Y)$  with standard Pareto margins, they assume

$$\Pr(X > t^\beta, Y > t^\gamma) = L(t; \beta, \gamma) t^{-\kappa(\beta, \gamma)}, \quad \beta, \gamma \geq 0, \quad \max(\beta, \gamma) > 0, \quad (2.1)$$

as  $t \rightarrow \infty$ , where  $\kappa(\beta, \gamma) \geq \max(\beta, \gamma)$  is a homogeneous function of order 1, i.e.  $\kappa(c\beta, c\gamma) = c\kappa(\beta, \gamma)$  for  $c > 0$ , and  $L(\cdot; \beta, \gamma)$  is a slowly varying function at infinity. The function  $\kappa$  is the key quantity in determining the behaviour of the joint survivor probability given in Equation (2.1) and both AD and AI can be captured under this function, with AD implying the lower bound  $\kappa(\beta, \gamma) = \max(\beta, \gamma)$ . The homogeneity of  $\kappa$  means it suffices to consider its values on a simplex. Define  $\lambda(w) = \kappa(w, 1 - w)$  with  $w \in (0, 1)$ , which we term the angular dependence function; it follows that  $\kappa(\beta, \gamma) = (\beta + \gamma)\lambda\left(\frac{\beta}{\beta + \gamma}\right)$ . Moreover, this approach can be used to estimate joint survivor probabilities where only one variable is large by taking values of  $w$  close to 0 or 1.

Heffernan and Tawn (2004) propose a very general modelling tool for conditional probabilities. Following Keef et al. (2013), we assume that for  $(X, Y)$  with standard Laplace margins, there exist normalising functions  $a : \mathbb{R} \rightarrow \mathbb{R}$  and  $b : \mathbb{R} \rightarrow \mathbb{R}_+$  such that

$$\lim_{t \rightarrow \infty} \Pr[(Y - a(X))/b(X) \leq z, X - t > x \mid X > t] = G(z)e^{-x}, \quad (2.2)$$

for a non-degenerate distribution function  $G$ . Similarly to Wadsworth and Tawn (2013), this framework is able to capture both AD and AI, with AD arising when  $a(x) = x$  and  $b(x) = 1$ . This method is a flexible approach for modelling multivariate extremes and is not restricted to only regions where both variables are large. Note that one could also

condition on the event  $Y > t$  and assume the existence of normalising functions for the variable  $X$ .

For the models given in Equations (2.1) and (2.2), inference is non-parametric and semi-parametric respectively. For the former, through transformation to exponential margins, the function  $\lambda$  can be estimated pointwise using the Hill estimator (Hill, 1975). For the latter, the functions  $a$  and  $b$  are typically estimated parametrically, while the distribution function  $G$  is estimated non-parametrically.

Alongside these approaches, we note that there are many existing copula-based models that can theoretically capture both AD and AI, such as those given in Pauli and Coles (2002), Wadsworth et al. (2017) and Huser and Wadsworth (2019). These models seek to unify the two extremal dependence regimes and the case of AD does not represent a limit case for the latter two, which could be practically advantageous. However, they all require stronger assumptions about the form of parametric family for the bivariate distribution, reducing their flexibility and limiting their use in practice. As a result, we prefer instead to consider the more flexible models denoted in Equations (2.1) and (2.2).

### 3 Bivariate Return Curve Estimation

We now consider techniques for estimating return curves in practice. We begin by introducing theoretical results for return curves in Section 3.1. Naive implementation of methods would generally produce curves that fail to respect these results, but imposing them will typically improve estimation. Section 3.2 details how to perform marginal transformations. In Section 3.3, we present existing approaches for return curve estimation before introducing novel estimation techniques in Section 3.4.

### 3.1 Return Curve Properties

A careful consideration of the theory surrounding the joint survival function allows us to deduce several properties about the shape and magnitude of  $R(p)$  for a given  $p \in (0, 1)$ . We begin by noting the return curve is linked to the joint distribution function  $F_{X,Y}$  by the equation  $\Pr(X > x, Y > y) = 1 - F_X(x) - F_Y(y) + F_{X,Y}(x, y)$ , where  $F_X$  and  $F_Y$  denote the marginal distribution functions of  $X$  and  $Y$ , respectively. The joint distribution function can be expressed in terms of  $F_X$ ,  $F_Y$  and a copula  $C$  via  $F_{X,Y}(x, y) = C(F_X(x), F_Y(y))$ . Throughout this section, we make the assumption that the random vector  $(X, Y)$  has strictly continuous marginal distributions.

**Property 3.1.** *Let  $x_p := F_X^{-1}(1 - p)$  and  $y_p := F_Y^{-1}(1 - p)$  (the  $(1 - p)$ -th quantiles of  $X$  and  $Y$ , respectively). Then for  $(x, y) \in R(p)$ ,  $x \leq x_p$  and  $y \leq y_p$ .*

*Proof.* We have  $\Pr(X > x) \geq \Pr(X > x, Y > y) = p = \Pr(X > x_p)$  and hence  $x \leq x_p$ .  $\square$

This result bounds the coordinate values that can be observed on the return curve. Next, by considering the limit of the joint survivor function as one variable converges to the lower limit of the marginal support, we obtain the following result.

**Property 3.2.** *Let  $\text{supp}(F)$  denote the support of  $F$  and  $x_{\inf} := \inf\{\text{supp}(F_X)\}$ ,  $y_{\inf} := \inf\{\text{supp}(F_Y)\}$ . We have that*

$$\Pr(X > x, Y > y) = \begin{cases} \Pr(Y > y) & \text{if } x \leq x_{\inf} \\ \Pr(X > x) & \text{if } y \leq y_{\inf} \end{cases}.$$

Combining this statement with Property 3.1, Property 3.3 follows.

**Property 3.3.** *Let  $(x, y) \in R(p)$ . If  $x \leq x_{\inf}$  ( $y \leq y_{\inf}$ ), then  $y = y_p$  ( $x = x_p$ ).*

These results allow us to easily compute the curve coordinates on the regions  $(-\infty, x_{inf}) \times (y_p, \infty)$  and  $(x_p, \infty) \times (-\infty, y_{inf})$ , assuming we can accurately estimate the marginal quantiles  $(x_p, y_p)$  and the infima of marginal supports  $(x_{inf}, y_{inf})$ . Finally, by comparing coordinates at different points on a return curve, we obtain the following result.

**Property 3.4.** *Suppose the copula,  $C$ , of  $(X, Y)$  on uniform margins has joint support on the whole of  $[0, 1]^2$  and let  $c$  denotes its density function. Given  $(x_1, y_1), (x_2, y_2) \in R(p)$  with  $0 < F_X(x_1), F_X(x_2) < 1$  and  $0 < F_Y(y_1), F_Y(y_2) < 1$ , we have that  $x_1 < x_2 \Leftrightarrow y_1 > y_2$ .*

*Proof.* Suppose  $x_1 < x_2$  and  $y_1 \leq y_2$ . This implies that

$$\begin{aligned}
p &= \Pr(X > x_1, Y > y_1) = \Pr(F_X(X) > F_X(x_1), F_Y(Y) > F_Y(y_1)) \\
&= \int_{F_X(x_1)}^1 \int_{F_Y(y_1)}^1 c(u, v) dv du \\
&= \int_{F_X(x_1)}^{F_X(x_2)} \int_{F_Y(y_1)}^1 c(u, v) dv du + \int_{F_X(x_2)}^1 \int_{F_Y(y_1)}^1 c(u, v) dv du \\
&> \int_{F_X(x_2)}^1 \int_{F_Y(y_1)}^1 c(u, v) dv du \quad (\text{since we have support on the whole of } [0, 1]^2) \\
&\geq \int_{F_X(x_2)}^1 \int_{F_Y(y_2)}^1 c(u, v) dv du = \Pr(X > x_2, Y > y_2) = p
\end{aligned}$$

implying  $p > p$ , a contradiction. Hence,  $y_1 > y_2$ . □

This result governs the shape of the contour defined by the return curve set. We note there is an alternative proof given in Cooley et al. (2019) under the assumption of monotonicity of the joint survivor function.

## 3.2 Marginal transformations

From Section 2, it is clear that in order to apply multivariate extreme value models, we need to standardise the marginal distributions of a random vector to a variety of different forms. For simulated data, where the true margins are known, this is not an issue since

bivariate observations can be transformed to any common marginal distribution using the PIT. However, in a practical setting, it is unlikely the true margins will be known and we therefore require a means to estimate them. Typically, inference involves two steps: forward transformation to get the data onto desired margins and back transformation to move any computed statistics, such as a return curve, back onto the original margins. For both steps, we use the semi-parametric approach given in Heffernan and Tawn (2004). Given an i.i.d. sample  $\{(x_i, y_i) : i = 1, \dots, n\}$  from a random vector  $(X, Y)$  with an unknown margins, we estimate the marginal distribution  $\hat{F}_X$  (similarly  $\hat{F}_Y$ ) by

$$\hat{F}_X(x) = \begin{cases} 1 - \{1 - \tilde{F}_X(u_X)\}\{1 + \xi_X(x - u_X)/\sigma_X\}_+^{-1/\xi_X} & \text{for } x > u_X, \\ \tilde{F}_X(x) & \text{for } x \leq u_X, \end{cases} \quad (3.1)$$

where the first line represents the GP distribution above a high threshold  $u_X$  and  $\tilde{F}_X$  is the empirical distribution given by  $\tilde{F}_X(x) = \sum_{i=1}^n \mathbb{1}(x_i \leq x)/(n+1)$ . This approach ensures the marginal tail behaviour is captured within the transformation. Moreover, Equation (3.1) can be easily inverted to perform the back transformation step. To be able to compare curve estimates from data sets, we require a common choice of margins. For this article, we select standard exponential margins; this allows us to easily define uncertainty quantification and diagnostic tools for return curves, as discussed in Section 4.

### 3.3 Existing Methodology

Recall that the goal is to estimate curves for small probabilities. Since this requires extrapolation outside of the sampled data range, the most appropriate approach is to utilise asymptotically motivated models for the tail of a joint distribution, i.e., models based on extreme value theory. Whilst curve estimation methods exist which do not take this approach, we have chosen to focus only on those that do.

For our purpose, we define two categories of extreme value based approaches: flexible and non-flexible. We say an approach is non-flexible if it assumes explicit forms of the extremal dependence structure and/or parametric models for the copula distribution. A range of non-flexible approaches are available for estimating return curves, for example Stephenson (2002), Salvadori and De Michele (2004) and Marcon et al. (2017). These approaches often assume the copula is given by a BEV distribution, thereby implying the process exhibits AD. The necessity for making such a strict assumption is a well known drawback of this kind of multivariate extreme value model, since it is unlikely the form of extremal dependence will be known prior to analysis and AI is frequently observed in practice (Heffernan and Tawn, 2004; Huser and Wadsworth, 2019). Furthermore, the use of explicit parametric forms for the joint tail behaviour incurs strong modelling assumptions, reducing applicability of such approaches in practice.

A non-flexible technique that does not assume a parametric form for the copula is given in Cooley et al. (2019). The extremal return curve estimates are obtained by ‘projecting’ empirical curves estimated for less extreme probabilities. This approach treats the dependence regimes AD and AI separately. For AD, given a random vector  $(X, Y)$  with standard Fréchet margins, the following property of multivariate regular variation is exploited to obtain curve estimates (Resnick, 1987). Given two small probabilities  $p$  and  $p^*$  with  $p^* > p$ , multivariate regular variation implies that  $R(p) \approx s^{-1}R(p^*)$ , where  $s := p^*/p > 1$ . Here,  $R(p^*)$  is estimated empirically and scaled by the coefficient  $s^{-1}$  to produce an estimate for  $R(p)$ . A similar estimation procedure is proposed for AI based on the assumption of hidden regular variation (Resnick, 2002). However, as mentioned in Section 2, this approach only works in regions where both variables are large. To account for this, Cooley et al. (2019) proposed an ad-hoc procedure to link this region to the marginal axes. In Section 5, we compare the resulting curve estimates from this approach to novel estimation techniques introduced in this paper and show that even when the true extremal dependence structure

is known, the novel techniques we present consistently outperform this method.

Very few flexible approaches exist within the available literature; this is in part because the bivariate extreme value methodologies that allow for flexible estimation are relatively modern. Of the flexible methods that exist, the majority use a semi-parametric implementation of the conditional extremes model described in Equation (2.2) (Jonathan et al., 2014; Gouldby et al., 2017; Simpson and Wadsworth, 2017). However, like the other techniques introduced here, little to no consideration is given to the theory behind return curves, as discussed in Section 3.1. These theoretical results are likely to improve the quality of curve estimates from this model by ensuring curve values do not exceed marginal limits and the resulting curves have the correct shape.

To the best of our knowledge, the modelling techniques discussed here cover the majority of proposed methods for estimating return curves at extremal probabilities, demonstrating the sparseness of literature on this topic. Furthermore, we know of no attempt to compare curve estimates from these different methods. No formal or robust quantifications of return curve uncertainty or bias have been proposed previously, making it difficult to evaluate performance over different dependence structures. This is in part because return curves have two components in which the estimates can vary. As such, there does not exist a trivial extension of the frameworks for capturing uncertainty and bias in the univariate setting. Many approaches (Simpson and Wadsworth, 2017; Cooley et al., 2019) instead provide bootstrap curve estimates which, while representing the uncertainty in curve estimates, do not provide a formal quantification and hence cannot be used for the construction of confidence intervals or median curve estimates.

Alongside this issue, there is only one diagnostic tool in the literature for evaluating the accuracy of return curve estimates (Cooley et al., 2019). This tool utilised the result that, if data are i.i.d., the number of points in each survival region on the return curve should theoretically be  $\text{Binomial}(n, p)$  distributed, where  $n$  denotes the size of the data set. This

property can be used to construct a confidence region for the probability  $p$  and this region is compared to empirical survival probabilities. While the authors show that the majority of empirical probabilities appear to lie within the constructed confidence region, they fail to account for the sampling uncertainty and there is little discussion as to the accuracy of this tool for different values of  $n$  and  $p$ .

### 3.4 Novel methods for return curve estimation

#### 3.4.1 Method based on the approach given in Heffernan and Tawn (2004)

Let  $(X, Y)$  denote a random vector with standard exponential margins. In this section, we propose a novel implementation of the Heffernan and Tawn (2004) model which builds on the existing methods while incorporating the properties introduced in Section 3.1. These properties allow us to obtain more accurate curve estimates by bounding the values in the return curve sets and ensuring a valid shape is obtained. Since we are working on standard exponential margins, for which the marginal support is given by the set  $\mathbb{R}_+$ , we can immediately deduce from Property 3.1 that the coordinates of the return curve intersecting the margins are given by  $(0, y_p)$  and  $(x_p, 0)$ , with  $y_p = x_p = -\log(p)$  (the  $(1-p)$ -th quantile). These coordinates give us ‘start’ and ‘end’ points for curve construction.

Let  $(X_L, Y_L)$  denote that same vector on standard Laplace margins and suppose we wish to obtain a return curve estimate for a small probability  $p$ . For this, we fit the Heffernan and Tawn (2004) model twice, conditioning on both  $X_L$  and  $Y_L$  separately, thus allowing us to estimate the curve in different regions. In particular, we consider the regions defined by  $\{(x_L, y_L) \in \mathbb{R}^2 \mid y_L > x_L\}$  and  $\{(x_L, y_L) \in \mathbb{R}^2 \mid y_L \leq x_L\}$ , which we label regions 1 and 2 respectively.

For region 1, we first select a high quantile  $u_{Y_L}$  from the marginal distribution of  $Y_L$  such that  $\Pr(Y_L > u_{Y_L}) > p$ . For every data set considered within this paper, we selected the 0.95



quantile of this distribution; all return curve probabilities considered are smaller than 0.05. We assume the normalising functions are given by  $a(y) = \alpha y$  and  $b(y) = y^\beta$  for constants  $\alpha \in [-1, 1]$  and  $\beta \in (-\infty, 1)$ . As noted in Keef et al. (2013), these functions capture the limiting dependence structures for a wide range of distributions. The parameters  $\alpha$  and  $\beta$  can be estimated under the working assumption that the distribution function  $G$ , which captures the stochastic behaviour of the variable  $(X_L - \alpha Y_L)/Y_L^\beta \mid Y_L > u_{Y_L}$ , is normally distributed. We denote the fitted values by  $\hat{\alpha}$  and  $\hat{\beta}$ .

We then consider a sequence of high quantiles from  $Y_L$  that exist in the interval  $(u_{Y_L}, F_{Y_L}^{-1}(1 - p))$ . The upper end point of this interval is a limit on values  $Y_L$  can attain on this curve and the lower end point represents the minimal quantile for which the fitted model is valid. We denote this set by  $\mathcal{Y}$ , ordered such that the quantiles go from highest to lowest. Iteratively, we consider each  $y_* \in \mathcal{Y}$  in turn and let  $q := \Pr(Y_L > y_*)$ . Using the fitted parameter values, we use the model to simulate from the conditional distribution  $X_L \mid Y_L > y_*$ . Letting  $x_*$  denote the (estimated)  $(1 - p/q)$ -th quantile from this distribution, we have that the resulting coordinate  $(x_*, y_*)$  is a member of the set  $R_{(X_L, Y_L)}(p)$  since  $\Pr(X_L > x_*, Y_L > y_*) = \Pr(X_L > x_* \mid Y_L > y_*)\Pr(Y_L > y_*) = \frac{p}{q} \times q = p$ . We continue in this manner until we obtain a value  $x_{**}$  with  $y_* \leq x_{**}$  and  $y_* \in \mathcal{Y}$  or we have exhausted all values in the set  $\mathcal{Y}$ . The resulting coordinate set then gives an estimate of the curve in region 1.

A near identical procedure is used to obtain the curve estimate in region 2, this time selecting a high quantile  $u_{X_L}$  from the distribution of  $X_L$  and fitting the conditional model above this quantile. We then consider a set of quantiles in the region  $(x'_{**}, F_{X_L}^{-1}(1 - p))$ , where  $x'_{**} = x_{**}$  if  $x_{**}$  exists and  $u_{X_L}$  otherwise. We label this set  $\mathcal{X}$ , ordered such that the quantiles go from lowest to highest, and use the fitted model to obtain quantiles from the conditional distribution  $Y_L \mid X_L > x_*$  for each  $x_* \in \mathcal{X}$ . The resulting coordinate sets from both regions can then be combined to obtain an estimate of the return curve over

the entire joint support of  $(X_L, Y_L)$ . We once again apply the PIT to transform this curve estimate back to standard exponential margins, where the coordinates are combined with the ‘start’ and ‘end’ points deduced from Property 3.1. Finally, we consider the estimated set as a function of  $x$  and apply the result from Property 3.4 to ensure the resulting curve estimate is of the correct shape.

We note that the implementation of this model to estimate return curves is more complex than the methods proposed in Section 3.4.2 and Cooley et al. (2019). This is due to the fact the model requires a variable to condition on, meaning we have to fit the model twice. This makes constructing a return curve estimate more challenging since we require a means to join the point estimates obtained by conditioning on the  $Y$  variables to those obtained by conditioning on  $X$ .

### 3.4.2 Method based on the approach given in Wadsworth and Tawn (2013)

We also propose a novel implementation of the model described in Equation (2.1) to generate non-parametric return curve estimates. Given a random vector  $(X, Y)$  with standard exponential margins, we use the equivalent model representation given in Wadsworth and Tawn (2013): for any  $w \in (0, 1)$  and  $t > 0$ , we have

$$\Pr \left( T_w > t + u \mid T_w > u \right) \rightarrow \exp\{-t\lambda(w)\} \quad \text{as } u \rightarrow \infty,$$

where  $T_w := \min \left\{ \frac{X}{w}, \frac{Y}{1-w} \right\}$ . This implies that, for a large threshold  $u$ , the variable  $T_w - u \mid T_w > u$  is exponentially distributed with rate parameter  $\lambda(w)$ , allowing the angular dependence function to be estimated pointwise using the Hill estimator (Hill, 1975). Under this representation, one can obtain return curve estimates in a similar manner to the approach given in Cooley et al. (2019). For a small probability  $p$ , we select  $p^* > p$  and estimate the  $(1 - p^*)$ -th quantile of  $T_w$ , implying  $\Pr(T_w > u) = p^*$ . One can then find the

value of  $t > 0$  such that  $\Pr(T_w > t + u) = p$  since

$$p = \Pr(T_w > t + u) = \Pr(T_w > u) \times \Pr(T_w > t + u \mid T_w > u) = p^* \exp\{-t\lambda(w)\},$$

implying  $t = -\frac{1}{\lambda(w)} \log(p/p^*)$ . Setting  $(x, y) := (w(t + u), (1 - w)(t + u))$ , we have  $(x, y) \in R(p)$ . We repeat this procedure for a set of  $w \in (0, 1)$ , which we denote  $\mathcal{W}$ . This set is ordered such that the  $w$  values go from lowest to highest. For each  $w \in \mathcal{W}$ , we use the 95% empirical threshold of the variable  $T_w$  to obtain an estimate of the angular dependence function, which we denote  $\hat{\lambda}(w)$ . This estimate is then used to obtain point estimates in  $R(p)$ . Finally, similarly to the method in Section 3.4.1, we apply Properties 3.1 and 3.4.

## 4 Novel Tools for Return Curve Estimation

### 4.1 Quantifying Uncertainty for Return Curve Estimates

Previously proposed methods for return curve estimation have given little consideration to the problem of quantifying uncertainty and, crucially, do not offer a means to construct confidence regions for return curves (Simpson and Wadsworth, 2017; Cooley et al., 2019). Here, we propose a new method for capturing uncertainty in return curve estimates that addresses issues in the existing methods and provides a robust technique for comparing curve estimates from different models where the truth is known. We also consider the challenge of defining bias in this setting which, to the best of our knowledge, has not been previously discussed within the literature.

Let  $R(p)$  denote the true curve for the random vector  $(X, Y)$  and  $\hat{R}_{X,Y}(p)$  denote a model-based curve estimator. We say that this estimator is unbiased if

$$\mathbb{E}_{(x,y)} \left[ \hat{R}_{X,Y}(p) \right] = R(p), \quad (4.1)$$

where  $\mathbb{E}_{(x,y)}[\cdot]$  denotes the expectation over the joint distribution of  $(X, Y)$ . In any analysis, it is desirable to obtain an estimator with this property and also be able to quantify bias in the case where (4.1) does not hold.

Our goal is to define some type of confidence region for return curves at a given significance level  $\alpha \in (0, 1)$ . Since these curves vary in two dimensions, careful consideration is needed to ensure the resulting region represents  $\alpha$  in an intuitive and logical manner.

Figure 3 displays  $n = 10000$  datapoints from inverted logistic (Ledford and Tawn, 1997) and asymmetric logistic (Tawn, 1988) copulas on standard exponential margins. The true return curves for  $p = 1/10000$  are given in red while the curves estimated using the Wadsworth and Tawn (2013) model are given in green. A representation of sampling uncertainty will help to determine the quality of these estimates.

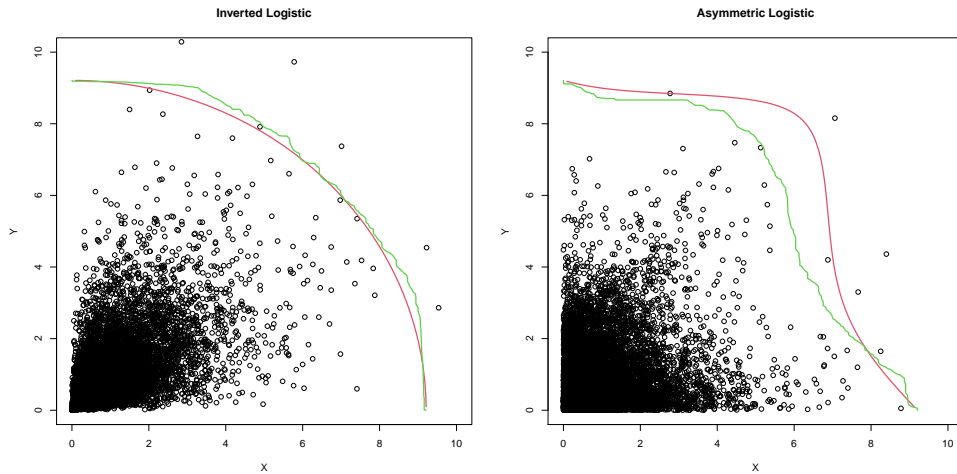


Figure 3: Estimated (green) vs true (red) curves for data sets simulated from inverted logistic (left) and asymmetric logistic (right) copulas.

To achieve this, we propose the following tool. On standard exponential margins, the joint support is given by the set  $\mathbb{R}_+^2$ ; we therefore select a set of decreasing positive gradients  $\mathcal{G} := \{g_j : 1 \leq j \leq m, g_j > 0 \forall j\}$  for some large  $m \in \mathbb{N}$ , with  $g_j \rightarrow \infty$  and  $g_j \rightarrow 0^+$  as  $j \rightarrow 1^+$  and  $j \rightarrow m^-$ , respectively. For each gradient  $g_j \in \mathcal{G}$ , we then consider the corresponding line intersecting the origin  $(0, 0)$  defined by the equa-

tion  $y = g_j x$ . The set  $\mathcal{G}$  is chosen such that the angles between adjacent gradient are equal; this is illustrated further in the supplementary material. Each line will intersect the estimated and true return curves exactly once, hence each gradient represents a common feature of both curves. Using this observation, we reformulate the definition of a return curve in terms of a positive gradient and a corresponding  $L_2$  (Euclidean) norm for  $(X, Y)$ . Let  $(x_g, y_g)$  denote the point on the true return curve intersecting the line defined by a gradient  $g > 0$  and define  $d_g := |x_g^2 + y_g^2|^{1/2}$  (the  $L_2$  norm from the origin to this point). The  $p$ -probability return curve is equivalently given by the set  $R(p) = \left\{ g \in [0, \infty), d_g \in (0, \infty) \mid \Pr \left( X > \sqrt{d_g^2/(1+g^2)}, Y > \sqrt{g^2 d_g^2/(1+g^2)} \right) = p \right\}$ . Therefore, uncertainty in estimated return curves can be quantified using the distribution of  $L_2$  distances for any given gradient. We propose the following bootstrap procedure: for  $k = 1, \dots, K$ ,

1. Bootstrap the original data sample to produce a new sample of the same size.
2. For each  $g_j \in \mathcal{G}$ , obtain estimates of the curve points and resulting  $L_2$  norm using the given model. Denote these values by  $(\hat{x}_{g_j,k}, \hat{y}_{g_j,k})$  and  $\hat{d}_{g_j,k}$ , respectively.

Given  $g_j \in \mathcal{G}$ , we construct empirical estimates of the mean, median, and  $100(1 - \alpha)\%$  confidence intervals for the norm value using the sample  $\{\hat{d}_{g_j,k} \mid 1 \leq k \leq K\}$ . Taking  $\alpha = 0.95$ , we estimate the 2.5% and 97.5% quantiles using this sample, which we denote  $\hat{d}_{g_j}^{0.025}$  and  $\hat{d}_{g_j}^{0.975}$  respectively. Assuming unbiased estimation,  $\Pr(\hat{d}_{g_j}^{0.025} \leq d_{g_j} \leq \hat{d}_{g_j}^{0.975}) \approx 0.95$  for sufficiently large  $K$  and hence one can show that

$$\Pr \left[ (x_{g_j}, y_{g_j}) \in \left\{ (x, y) \in \mathbb{R}_+^2 \mid d_{g_j} \in [\hat{d}_{g_j}^{0.025}, \hat{d}_{g_j}^{0.975}] \right\} \right] \approx 0.95,$$

implying the set  $\left\{ (x, y) \in \mathbb{R}_+^2 \mid d_{g_j} \in [\hat{d}_{g_j}^{0.025}, \hat{d}_{g_j}^{0.975}] \right\}$  defines a confidence region for estimated curve points along the line  $y = g_j x$ . Taking the maximum and minimum  $x$  and  $y$  coordinates

in this set, we obtain a rectangular confidence region for each gradient. These values, along with the  $x$  and  $y$  coordinates corresponding to the mean and median norm estimates, can be joined together in order of gradient to construct estimates of the mean, median, and 95% confidence intervals for the return curve.

We note that this procedure bears many similarities to the approach introduced in Haselsteiner et al. (2019) to characterise uncertainty of environmental contours. They also consider lines starting at a defined origin and the corresponding points of intersection for each line on an estimated contour and use bootstrapping to construct median and confidence interval estimates of the contour. However, the ethos behind our proposed tool differs in two ways. Firstly, environmental contours and return curves have different definitions and are only equal in a limited number of cases (Haselsteiner et al., 2021). This suggests what is proposed for these contours may not be appropriate in the context of return curves. Furthermore, the development of environmental contours is solely motivated by practical problems whereas our approach is developed in a more general, theoretical setting. Consequently, the focus and goals of these approaches are not the same and hence cannot be easily compared.

Our procedure is illustrated in Figure 4 for both copulas examples, with  $|\mathcal{G}| = 150$ . The confidence interval width appears to vary with the gradient in both cases. For the inverted logistic copula, the true curve is captured by the estimated confidence region at all gradients; this is what we would expect, since the model proposed in Wadsworth and Tawn (2013) is exact for this particular example. For the asymmetric logistic copula, the estimated confidence interval only contains the true curve in certain regions of the  $\mathbb{R}_+^2$  plane. This observation suggests potential bias in curve estimates for this particular model.

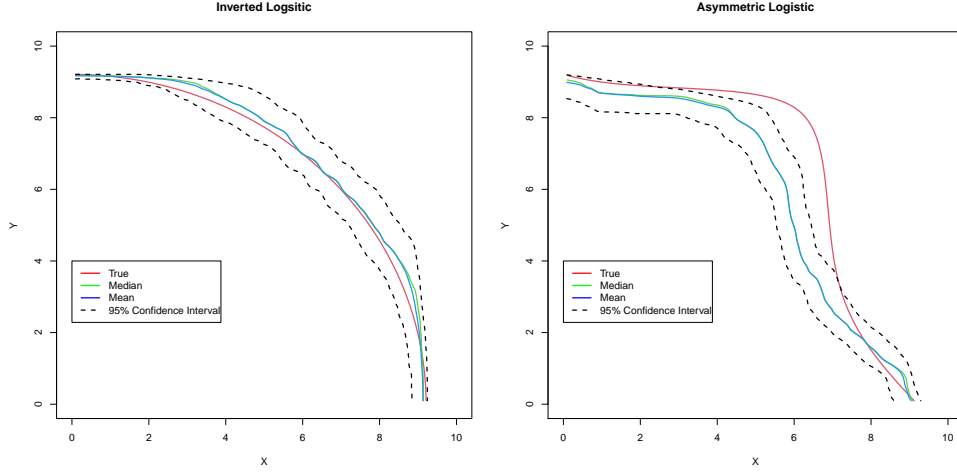


Figure 4: Comparison of median, median, and 95% confidence interval return curve estimates (green, blue and black dotted lines respectively) to the true return curves (red) for inverted logistic (left) and asymmetric logistic (right) copulas with  $K = 1000$  bootstraps.

## 4.2 Return Curve Diagnostic Tool

Since the true return curve is unknown in practice, we require of means of evaluating the goodness of fit for a curve estimate,  $\hat{R}(p)$ , from a particular sample. We propose such a technique and illustrate the method using an example data set simulated from a logistic copula (Tawn, 1988) on standard exponential margins.

Consider the shaded survival regions defined in the left panel Figure 5 for an estimated return curve  $\hat{R}(p)$ , where  $p$  is small but  $\hat{R}(p)$  is in the range of the data. Three regions of the form  $(x, \infty) \times (y, \infty)$  are illustrated for three points on the curve  $(x, y)$ . The probability of lying within each such region should equal  $p$ .

To assess this, we consider the survival regions for a chosen subset of points on the estimated curve. For convenience, this subset is chosen such that points correspond to a set of decreasing positive gradients  $\mathcal{G}$ . This results in the set of points sufficing as a representation of the estimated curve, as demonstrated in the figure. If this estimated curve accurately reflects the true return curve, the empirical probability of observing data within each survival region along the curve should be close to  $p$ . For an index  $1 \leq j \leq m$ ,

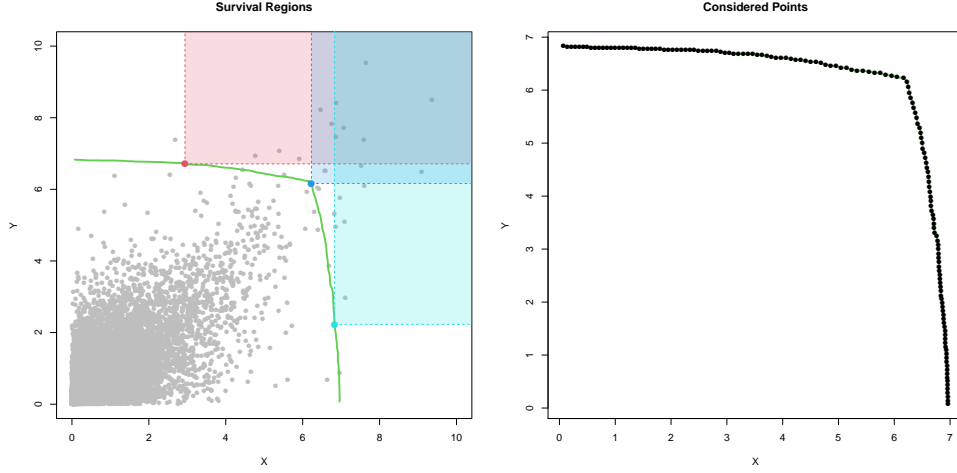


Figure 5: Left: Survival regions for three points on the estimated return curve. Right: Subset of points on the estimated curve considered in diagnostic.

let  $(\hat{x}_j, \hat{y}_j)$  denote the corresponding point on  $\hat{R}(p)$  and let  $(\mathbf{x}, \mathbf{y}) = \{(x_i, y_i) : 1 \leq i \leq n\}$  denote the observed sample that has been used to estimate the curve. The empirical estimate, which we denote  $\hat{p}_j$ , is given by the proportion of points lying in the region  $(\hat{x}_j, \infty) \times (\hat{y}_j, \infty)$ . We then apply the bootstrap to resample the original data set and this estimation procedure is repeated to obtain a range of empirical estimates. For each  $j$ , we let  $\hat{\mathcal{P}}_j$  denote the set of empirical probability estimates obtained using bootstrapping. Finally, we estimate the median and 95% pointwise confidence intervals for each  $j$  by taking empirical 2.5%, 50% and 97.5% quantiles of the set  $\hat{\mathcal{P}}_j$ . These estimates can be stitched together by index order to represent the diagnostic over the whole curve.

This procedure is illustrated in Figure 6 using the example given in Figure 5. The black line and shaded regions in the figure represent the empirical estimates of the median and 95% pointwise confidence intervals, respectively, for each index, with the red line denoting the true probability. As can be observed, for all indices, the confidence bounds contain the true value  $p$ , suggesting this estimated curve accurately represents this value once uncertainty is accounted for. However, the median empirical estimates are greater than  $p$  at the majority of indices, suggesting a slight overestimation bias for this particular curve



estimate.

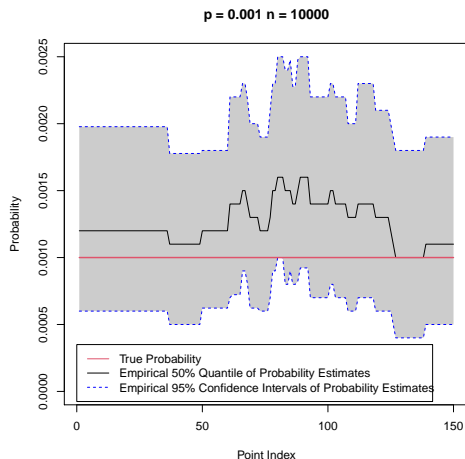


Figure 6: Illustration of diagnostic tool. Solid red and black lines denotes true and mean empirical estimates, respectively, and grey shaded region between dotted blues lines describe empirical 95% CI estimates.

This tool provides a means to assess the accuracy of a given curve estimate for a data set with no knowledge of marginal or copula distributions. However, the main limitation of this framework is the fact extreme survival region probabilities are estimated empirically. The accuracy of such estimates will therefore be directly related to the sample size  $n$  and the probability  $p$ . This represents a broader problem within the extremes literature, since, by definition, we will observe very few extremes values that can be used verify and justify a given approach. This issue is illustrated further in the supplementary material, where we consider decreasing probabilities for a fixed sample size. The utility of the tool reduces as the value of  $p$  decreases, with all empirical probability estimates equal to 0 for the smallest probability. However, as is common within such an analysis, if the tool appears to illustrate goodness of fit for the data at less extreme probabilities, we can more rigorously justify extrapolating to more extreme values.

We note that the confidence intervals produced through bootstrapping for the return curves in Section 4.1, and survival probabilities in Section 4.2, are all pointwise and dependent across the index sets. Although they cannot be interpreted across the whole range,

they still provide a useful assessment of the utility of various models.

## 5 Simulation Study

In this section, we compare return curve estimates from the models discussed in Section 3.4 to those estimated using the methodology of Cooley et al. (2019). For this, we consider several simulated data sets on standard exponential margins, representing a range of different extremal dependence structures. Specifically, we consider the following copula families: BEV copulas from logistic and asymmetric logistic families, the bivariate normal copula with correlation coefficient  $\rho$ , inverted BEV copulas from logistic and asymmetric logistic families, the bivariate t copula with correlation coefficient  $\rho$  and degrees of freedom  $\nu$  and the Frank copula with dependence parameter  $\theta$ .

For the methods introduced in Cooley et al. (2019), we transform the data to standard Fréchet margins, use the procedures proposed in the paper to obtain return curve estimates, transform back to standard exponential margins and apply Properties 3.1 and 3.4. For any example, the chosen estimation procedure is determined by the extremal dependence exhibited by the underlying copula. The fact this must be specified prior to inference illustrates a drawback of this approach, since the extremal dependence structure is rarely known in practice. The code for implementing this approach can be found at <https://www.stat.colostate.edu/~cooleyd/Isolines/>.

For every model, the appropriate procedures are used to obtain estimates of exactly 200 points on the return curve, which are then connected to the ‘start’ and ‘end’ points. This way, we can do a fair comparison of the resulting estimates since all curves will have point estimates in a variety of regions on the  $\mathbb{R}_+^2$  plane.

Examples of both estimated and true return curves for each copula, with  $n = 10000$  and  $p = 10^{-3}$ , are illustrated in Figure 7. The figure suggests some possible shortcomings

within estimates obtained using the Cooley et al. (2019) approach, as the curve estimates for the second, eighth and ninth examples do not appear to capture the behaviour of the corresponding true curves. We also note that for the Frank copula, there is a distinctly ‘linear’ segment of the curve estimate from the Heffernan and Tawn (2004) model. This lack of fit reflects a shortcoming of this approach for data sets with negative dependence.

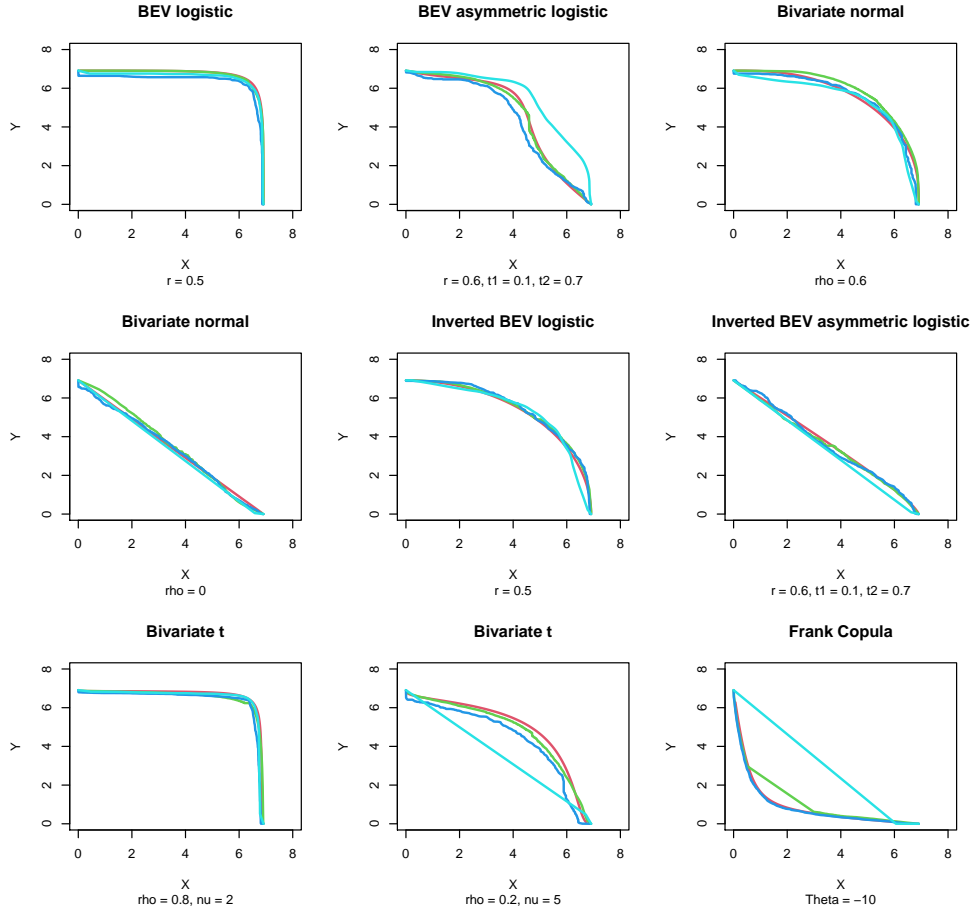


Figure 7: Examples curve estimates for each copula family. True curves are given in red while the estimated curves from the Heffernan and Tawn (2004), Wadsworth and Tawn (2013) and Cooley et al. (2019) models are given in green, dark blue and light blue, respectively.

For this study, we evaluated the bias and sampling uncertainty that arises from curve estimates for the models illustrated in Figure 7. To assess bias, 1000 samples of size  $n = 100000$  were simulated from each copula and the probabilities  $p = 10^{-3}$  and  $p = 10^{-4}$  were considered. Adapting the procedure detailed in Section 4.1, the median curves for

each copula were obtained over the 1000 samples and compared to the corresponding true curves. This median curve should provide an approximation of the expectation in Equation 4.1.

To summarise the results, we consider a plot of the  $L_2$  norm values for the true and estimated median curves at gradients  $g_j \in \mathcal{G}$  against the corresponding gradient indices  $j \in [1, |\mathcal{G}|]$ , where  $|\mathcal{G}| = 150$ . Numerical integration can then be used to compute the absolute area between the resulting norm curves. An illustration of this procedure can be found in the supplementary material.

The summary statistics for each copula-model pairing are given in Table 1. The bias from each model appears to vary significantly over the different copula structures, suggesting that the bias in return curve estimates exhibited by a particular model varies with the form of extremal dependence. It is clear that the bias from the Cooley et al. (2019) curve estimates are significantly larger for all but two of the copulas considered; in two cases where this approach performs well, the method has an unrealistic advantage, namely that the extremal dependence class has been correctly specified as AD. Overall, the bias appears significantly lower for the other two models, so we choose not to consider the approach of Cooley et al. (2019) further. On the other hand, the models proposed in Heffernan and Tawn (2004) and Wadsworth and Tawn (2013) appear to have similar amounts of bias for the majority of copula structures considered, and neither consistently outperforms the other.

To assess the sampling uncertainty from the remaining models, we compute the coverage for the estimated confidence regions. For this, 500 simulated samples of size  $n = 10000$  from each copula were considered. Using bootstrapping with  $K = 200$  iterations, return curve confidence regions were obtained following the procedure outlined in Section 4.1 for probabilities of  $p = 10^{-3}$  and  $10^{-4}$ , and we assessed the coverage of these at five fixed gradients, selected such that the coverage of the estimated curves could be evaluated for a

Table 1: Summary statistics for each model under different copula structures. In each case, 1000 samples of  $n = 100000$  datapoints were simulated and the median curves were computed for  $p = 10^{-3}$  and  $10^{-4}$ . ‘HT’, ‘WT’ and ‘CO’ correspond to the median curve estimates from the Heffernan and Tawn (2004), Wadsworth and Tawn (2013) and Cooley et al. (2019) models, respectively.

Copula	Model	$p = 10^{-3}$			$p = 10^{-4}$		
		HT	WT	CO	HT	WT	CO
BEV Logistic		1.80	10.83	0.26	2.56	14.07	0.22
BEV Asymmetric Logistic		23.61	28.27	83.40	47.66	78.16	124.49
Bivariate Normal 1		2.49	3.01	25.24	4.07	7.69	37.53
Bivariate Normal 2		0.18	0.14	9.91	0.37	0.22	3.34
Inverted BEV Logistic		2.75	0.39	26.27	4.06	0.56	34.67
Inverted BEV Asymmetric Logistic		0.80	0.19	36.02	1.22	0.30	27.95
Bivariate T 1		8.26	7.17	1.80	11.24	10.44	3.32
Bivariate T 2		14.62	26.37	158.89	39.77	74.95	187.72
Frank		46.39	9.65	394.87	30.33	46.56	506.58

variety of regions. Two of the gradients are only considered for the BEV asymmetric logistic and inverted BEV asymmetric logistic copulas, since these are the only distributions not to exhibit symmetry. We consider 95% confidence regions for both probabilities. The results for  $p = 10^{-3}$  are given in Table 2; the results for  $p = 10^{-4}$  can be found in the supplementary material, along with an illustration of the estimation procedure.

These coverage results provide an insight into differences in the Heffernan and Tawn (2004) and Wadsworth and Tawn (2013) models. Firstly, for gradients close to the margins, the coverage from the Wadsworth and Tawn (2013) model tends to be closer to the nominal level than that from the Heffernan and Tawn (2004) model. This is especially apparent when examining the scores at both probabilities for the logistic and first bivariate normal copula examples. We note that imposing Property 3.1 will affect the coverage near the margins, since we do not allow return curve coordinate estimates that exceed the marginal  $(1 - p)$ -th quantiles, resulting in constrained confidence intervals. We also note that the coverage values for the Frank copula from the Heffernan and Tawn (2004) framework are noticeably small; this relates to the aforementioned shortcoming of this approach for data sets with negative dependence. On the other hand, certain coverage values obtained using

the Wadsworth and Tawn (2013) approach are noticeably smaller than the corresponding values from the Heffernan and Tawn (2004) approach; for example, for the BEV asymmetric logistic copula at  $p = 10^{-4}$  and the second bivariate t copula.

On the whole, neither model consistently outperforms the other over the copulas and gradients considered and encouragingly, the resulting coverage scores were, in many cases, close to 0.95. Combined with the bias results, it appears that neither approach is obviously superior to the other and both give high quality return curve estimates. Since all models for multivariate extremes are based on asymptotic arguments which sometimes hold better for one data set than another; this conclusion is most likely a reflection of the different asymptotic arguments for the Heffernan and Tawn (2004) and Wadsworth and Tawn (2013) models. Therefore, from a practical point of view, we cannot easily distinguish between these methods and either model could be selected for return curve estimation.

## 6 Case Study

We now apply our techniques to two data sets of practical importance. The first contains air pollutant data from the centre of Leeds, UK. The data represent daily maxima of ozone and nitrogen dioxide recorded between 1994-2021, both measured in  $\mu\text{g}/\text{m}^3$ . We restrict attention to the months of June-August only, since this is when the highest ozone and nitrogen dioxide values occur and we do not need to account for seasonal behaviour for this subset. This results in  $n = 2269$  observations, which is an extension of the case study considered in Heffernan and Tawn (2004). Such measurements are important for a variety of reasons; for example, in the UK, the Air Quality Standards Regulations 2010 state that ozone and nitrogen dioxide should not exceed levels of  $120\mu\text{g}/\text{m}^3$  and  $200\mu\text{g}/\text{m}^3$ , respectively, on a regular basis (<https://www.gov.uk/government/statistics/air-quality-statistics/>). Whilst the primary pollutant nitrogen dioxide is a precursor for the secondary pollutant

Table 2: Coverage values for  $p = 10^{-3}$ . ‘HT’ and ‘WT’ correspond to the Heffernan and Tawn (2004) and Wadsworth and Tawn (2013) models, respectively.

Copula	Probability	$p = 10^{-3}$									
	Model	HT					WT				
BEV Logistic	Gradient	1	2	3	4	5	1	2	3	4	5
	Coverage	0.014	0.97	0.8	*	*	0.856	0.606	0.896	*	*
BEV Asymmetric Logistic	Gradient	1	2	3	4	5	1	2	3	4	5
	Coverage	0.756	0.938	0.868	0.86	0.896	0.908	0.054	0.362	0.902	0.936
Bivariate Normal 1	Gradient	1	2	3	4	5	1	2	3	4	5
	Coverage	0.358	0.942	0.956	*	*	0.872	0.93	0.912	*	*
Bivariate Normal 2	Gradient	1	2	3	4	5	1	2	3	4	5
	Coverage	0.948	0.93	0.955	*	*	0.93	0.934	0.934	*	*
Inverted BEV Logistic	Gradient	1	2	3	4	5	1	2	3	4	5
	Coverage	0.78	0.932	0.932	*	*	0.864	0.944	0.942	*	*
Inverted BEV Asymmetric Logistic	Gradient	1	2	3	4	5	1	2	3	4	5
	Coverage	0.96	0.929	0.942	0.951	0.922	0.924	0.934	0.958	0.942	0.904
Bivariate T 1	Gradient	1	2	3	4	5	1	2	3	4	5
	Coverage	0.504	0.928	0.512	*	*	0.92	0.758	0.884	*	*
Bivariate T 2	Gradient	1	2	3	4	5	1	2	3	4	5
	Coverage	0.784	0.896	0.93	*	*	0.938	0.806	0.632	*	*
Frank	Gradient	1	2	3	4	5	1	2	3	4	5
	Coverage	0.896	0	0	*	*	0.922	0.692	0.714	*	*

ozone, risks of extreme episodes in either pollutant are usually quantified separately. Estimating return curves for the two variables may provide useful insight into the joint extremal behaviour of these gases.

The second data set contains hourly measured wave data obtained from a buoy off the coast of Florida, USA. This data set was previously used in a benchmarking exercise for environmental contours (Haselsteiner et al., 2019). The variables considered are significant wave height (m) and zero up crossing period (s), with 10 years of hourly observations available, resulting in  $n = 83917$  observations. Such variables are of particular relevance for the reliability of offshore structures and contour estimates are commonly used to inform the design basis for such structures. Therefore, deriving extreme combinations of these variables may again provide useful information in a structural reliability context. Both data sets are illustrated (along with curve estimates) in Figure 8.

We firstly transform both data sets to standard exponential margins. Neither data set appears to exhibit strong seasonal, marginal trends, hence we assume the margins are identically distributed over time. We then apply the techniques from Section 3.4 to obtain curve estimates for probabilities of  $p = 10^{-3}$  (pollutants) and  $p = 10^{-4}$  (wave), approximately corresponding to return periods of 11 and 1 years, respectively.

The return curve estimates are then transformed back onto the original margins and the resulting curves are illustrated in Figure 8. For the gas data, large portions of each of the return curve estimates contain ozone values exceeding the government limit of  $120\mu g/m^3$ , while all estimated nitrogen dioxide values lay below the corresponding limit of  $200\mu g/m^3$ . The point where both limits are exceeded is outside the curve estimate, suggesting this event is rare.

Next, we apply the diagnostic tool introduced in Section 4.2. Both data sets exhibit marginal temporal dependence, therefore we use block bootstrapping when resampling. Block sizes of 30 and 200 were selected for the gas and wave data, respectively, by consider-



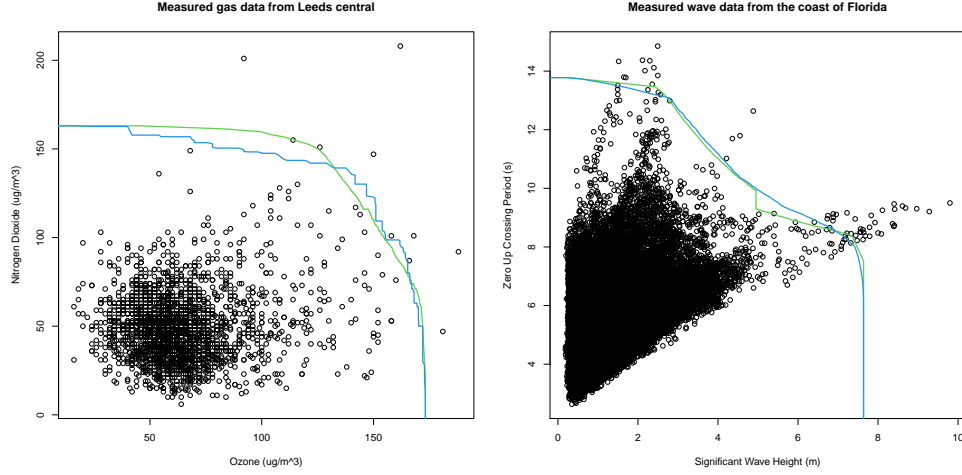


Figure 8: Return curve estimated for measured gas (left) with  $p = 10^{-3}$  and wave (right) data with  $p = 10^{-4}$ . Green and blue lines represent the estimates from the Heffernan and Tawn (2004) and Wadsworth and Tawn (2013) models, respectively.

ing plots of the autocorrelation function and selecting values beyond which the dependence appeared insignificant for both variables. These block sizes were then used to bootstrap the original data sets and a range of empirical probability estimates were obtained at various points, corresponding to a set of 150 positive gradients, for the curve estimates on the original margins. The resulting diagnostic plots for the gas and wave data sets are given in Figures 9 and 10, respectively.

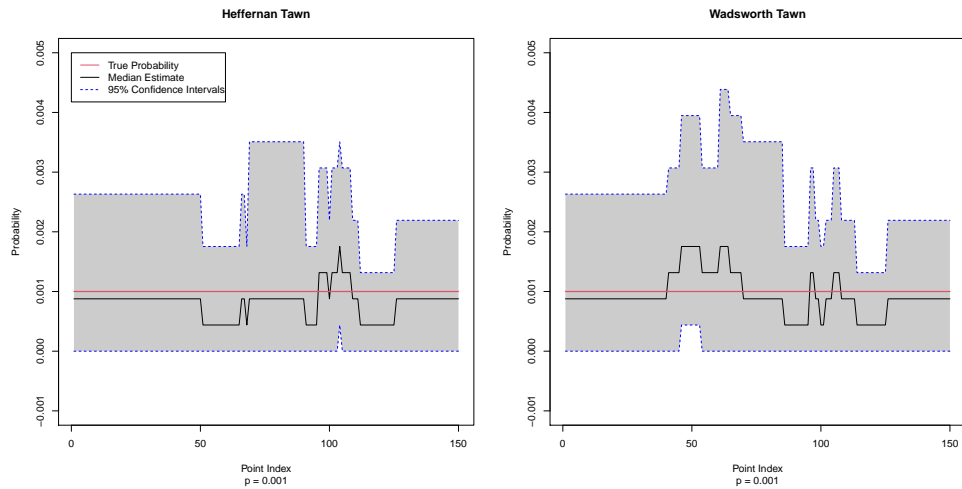


Figure 9: Gas data diagnostic plots with  $K = 1000$  block bootstraps from Heffernan and Tawn (2004) (left) and Wadsworth and Tawn (2013) (right) models, respectively.

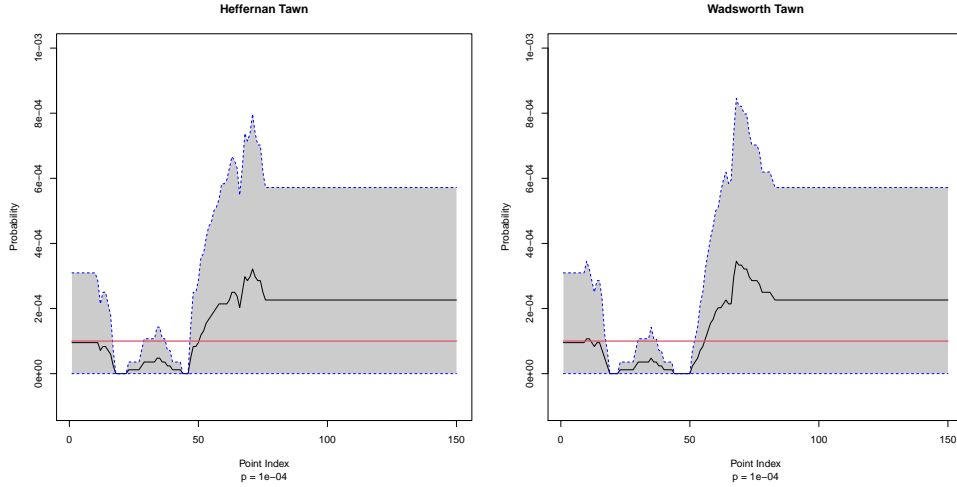


Figure 10: Wave data diagnostic plots with  $K = 1000$  block bootstraps from Heffernan and Tawn (2004) (left) and Wadsworth and Tawn (2013) (right) models, respectively.

For the gas data, Figure 9 suggests both models perform similarly and provide accurate curve estimates. For the wave data, Figure 10 again suggests that both models perform similarly, but the accuracy appears to vary depending on the index (equivalently the gradient), suggesting both models are more easily able to capture curve behaviour in certain regions.

Finally, we use the uncertainty quantification techniques introduced in Section 4.1 to obtain median and mean curve estimates, along with 95% confidence intervals. Due to ease of implementation and the similar performance of the models introduced in Section 3.4, we use the Wadsworth and Tawn (2013) approach to obtain estimates. The resulting curve estimates are illustrated in Figure 11; both estimated uncertainty regions appear sensible.

## 7 Discussion

We have considered the concept of a return curve as a general bivariate extension to a return level and introduced novel curve estimation techniques, illustrating that these methods produce estimates with less bias compared to an existing approach by Cooley et al. (2019). Furthermore, our methods offer flexibility since neither requires the form of extremal de-

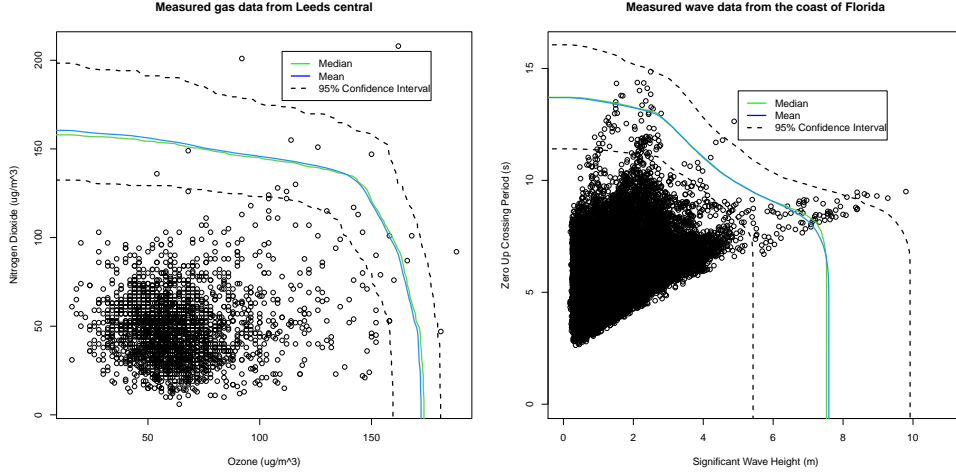


Figure 11: Median (green) and mean (blue) curve estimate, along with 95% (black dotted) confidence regions obtained using block bootstrapping with  $K = 250$  for the gas (left) and wave (right) data sets. The Wadsworth and Tawn (2013) model was used to obtain all estimates.

pendence to be pre-specified. This is an obvious advantage, since determining the extremal dependence structure is seldom straightforward. We have also proposed novel uncertainty quantification and diagnostic tools for the risk measure.

While we have focused on bivariate random vectors, both concepts and methodology can be extended to the general multivariate setting. However, higher dimensional curves would be difficult to visualise and capturing the dependence structures in higher dimensions becomes increasingly complex, since different two dimensional marginals can exhibit different forms of extremal dependence. Nevertheless, in the bivariate setting, we believe return curves are a useful tool for researchers to explore joint extremal behaviour and develop a better understanding of potential risks. Indeed return curves are already utilised to analyse risks for ocean and coastal structures. However, it is important to note these measures only denote the rarity of events, not impact. For example, from the left panel of Figure 11, one can observe points ‘below’ (to the south west) the estimated return curve uncertainty region where ozone exceeds  $120\mu g/m^3$ . Therefore, in practice, researchers must carefully consider which regions of the multivariate space are impactful prior to inference.

We have only considered a single type of risk measure in this article but different risk measures will likely be appropriate in different contexts. For the air pollutant data, for example, it may be more appropriate to consider alternative measures, such as the set given by  $\{(x, y) \in \mathbb{R}^2 \mid \Pr(X > x \text{ OR } Y > y) = p\}$ , which can be easily obtained from the return curve via the inclusion-exclusion formula. From Figure 8, we would expect this alternative set to contain several ozone values greater than  $120\mu\text{g}/\text{m}^3$ .

Throughout this paper, we assume data have i.i.d. margins. However, as noted in Section 6, the data sets both appear to exhibit marginal temporal dependence. We account for this using block bootstrapping to quantify uncertainty, but this creates the additional challenge of selecting a block size. For this, we use an ad-hoc technique based on examinations of ACF plots. An in-depth investigation could improve on this approach through a more robust, theoretically justified resampling scheme. In addition to temporal dependence, both data sets appear to exhibit weak marginal non-stationarity, possibly due to environmental changes over time. Accounting for this in the context of return curves presents many challenges, since return curves are defined in the stationary setting only and all models introduced in Section 3 assume i.i.d. data. While a range of approaches exist for capturing non-stationarity in the univariate setting (e.g. Eastoe, 2019), relatively few approaches exist in the multivariate setting. This motivates the development of novel ‘non-stationary’ return curves and techniques for capturing marginal and dependence trends, while also being able to quantify uncertainty in curve estimates. This is a topic of current research.

## Acknowledgements

This paper is based on work completed while Callum Murphy-Barltrop was part of the EPSRC funded STOR-i centre for doctoral training (EP/L015692/1).

## SUPPLEMENTARY MATERIAL

**Additional figures and tables.** File containing figures and a table that further illustrate ideas introduced in the article. (.pdf file)

**Code and data.** Zip file containing two R scripts and the case study data sets. Scripts can be used to reproduce bias and case study results from Sections 5 and 6, respectively. (.zip file)

## References

- Beirlant, J., Goegebeur, Y., Teugels, J., Segers, J., De Waal, D., and Ferro, C. (2004). *Statistics of extremes: Theory and applications*. John Wiley & Sons, Inc.
- Boldi, M. O. and Davison, A. C. (2007). A mixture model for multivariate extremes. *Journal of the Royal Statistical Society. Series B: Statistical Methodology*, 69(2):217–229.
- Coles, S. (2001). *An Introduction to Statistical Modeling of Extreme Values*. Springer Series in Statistics. Springer London, London.
- Coles, S. G. and Tawn, J. A. (1991). Modelling Extreme Multivariate Events. *Journal of the Royal Statistical Society. Series B: Statistical Methodology*, 53(2):377–392.
- Cooley, D., Thibaud, E., Castillo, F., and Wehner, M. F. (2019). A nonparametric method for producing isolines of bivariate exceedance probabilities. *Extremes*, 22(3):373–390.
- de Haan, L. and Resnick, S. I. (1977). Limit theory for multivariate sample extremes. *Zeitschrift für Wahrscheinlichkeitstheorie und Verwandte Gebiete*, 40(4):317–337.
- Eastoe, E. F. (2019). Nonstationarity in peaks-over-threshold river flows: A regional random effects model. *Environmetrics*, 30(5):1–18.

- Eckert-Gallup, A. and Martin, N. (2016). Kernel density estimation (KDE) with adaptive bandwidth selection for environmental contours of extreme sea states. *OCEANS 2016 MTS/IEEE Monterey, OCE 2016*, pages 1–5.
- Einmahl, J. H. and Segers, J. (2009). Maximum empirical likelihood estimation of the spectral measure of an extreme-value distribution. *Annals of Statistics*, 37(5 B):2953–2989.
- Environmental Agency (2005). CSG 15 Final Project Report. *Research Policy*, 15(May):1–11.
- Gouldby, B., Wyncoll, D., Panzeri, M., Franklin, M., Hunt, T., Hames, D., Tozer, N., Hawkes, P., Dornbusch, U., and Pullen, T. (2017). Multivariate extreme value modelling of sea conditions around the coast of England. *Proceedings of the Institution of Civil Engineers: Maritime Engineering*, 170(1):3–20.
- Haselsteiner, A. F., Coe, R. G., Manuel, L., Chai, W., Leira, B., Clarindo, G., Guedes Soares, C., Dimitrov, N., Sander, A., Ohlendorf, J.-h., Thoben, K.-d., Haute, G. D., Mackay, E., Jonathan, P., Qiao, C., Myers, A., Rode, A., Hildebrandt, A., Schmidt, B., and Vanem, E. (2021). *A benchmarking exercise for environmental contours (preprint from January 2021)*. Preprint.
- Haselsteiner, A. F., Nguyen, P. T., Coe, R. G., Martin, N., Manuel, L., and Eckert-Gallup, A. (2019). A benchmarking exercise on estimating extreme environmental conditions: Methodology and Baseline results. *Proceedings of the International Conference on Off-shore Mechanics and Arctic Engineering - OMAE*, 3:1–10.
- Heffernan, J. E. and Tawn, J. A. (2004). A conditional approach for multivariate extreme values. *Journal of the Royal Statistical Society. Series B: Statistical Methodology*, 66(3):497–546.

- Hill, B. M. (1975). A Simple General Approach to Inference About the Tail of a Distribution. *The Annals of Statistics*, 3(5):1163–1174.
- Huser, R. and Wadsworth, J. L. (2019). Modeling Spatial Processes with Unknown Extremal Dependence Class. *Journal of the American Statistical Association*, 114(525):434–444.
- Jonathan, P., Ewans, K., and Flynn, J. (2014). On the estimation of ocean engineering design contours. *Journal of Offshore Mechanics and Arctic Engineering*, 136(4):1–8.
- Keef, C., Papastathopoulos, I., and Tawn, J. A. (2013). Estimation of the conditional distribution of a multivariate variable given that one of its components is large: Additional constraints for the Heffernan and Tawn model. *Journal of Multivariate Analysis*, 115:396–404.
- Ledford, A. W. and Tawn, J. A. (1996). Statistics for near independence in multivariate extreme values. *Biometrika*, 83(1):169–187.
- Ledford, A. W. and Tawn, J. A. (1997). Modelling dependence within joint tail regions. *Journal of the Royal Statistical Society. Series B: Statistical Methodology*, 59(2):475–499.
- Manuel, L., Nguyen, P. T., Canning, J., Coe, R. G., Eckert-Gallup, A. C., and Martin, N. (2018). Alternative approaches to develop environmental contours from metocean data. *Journal of Ocean Engineering and Marine Energy*, 4(4):293–310.
- Marcon, G., Naveau, P., and Padoan, S. (2017). A semi-parametric stochastic generator for bivariate extreme events. *Stat*, 6(1):184–201.
- Mattei, J., Vial, E., Rebour, V., Liemersdorf, H., and Turschmann, M. (2001). Generic results and conclusions of re-evaluating the flooding protection in French and German nuclear power plants. *Eurosafe*, 1999.

- Office for Nuclear Regulation (2018). NS-TAST-GD-013 Revision 8. Technical report, Department for Work and Pensions.
- Pauli, F. and Coles, S. (2002). Models and inference for uncertainty in extremal dependence. *Biometrika*, 89(1):183–196.
- Ramos, A. and Ledford, A. (2009). A new class of models for bivariate joint tails. *Journal of the Royal Statistical Society. Series B: Statistical Methodology*, 71(1):219–241.
- Resnick, S. (2002). Hidden Regular Variation, Second Order Regular Variation and Asymptotic Independence. *Extremes*, 5(4):303–336.
- Resnick, S. I. (1987). *Extreme Values, Regular Variation and Point Processes*. Springer Series in Operations Research and Financial Engineering. Springer New York, New York.
- Rootzén, H. and Tajvidi, N. (2006). Multivariate generalized Pareto distributions. *Bernoulli*, 12(5):917–930.
- Ross, E., Astrup, O. C., Bitner-Gregersen, E., Bunn, N., Feld, G., Gouldby, B., Huseby, A., Liu, Y., Randell, D., Vanem, E., and Jonathan, P. (2020). On environmental contours for marine and coastal design. *arXiv*, 195:106194.
- Salvadori, G. and De Michele, C. (2004). Frequency analysis via copulas: Theoretical aspects and applications to hydrological events. *Water Resources Research*, 40(12):1–17.
- Serinaldi, F. (2015). Dismissing return periods! *Stochastic Environmental Research and Risk Assessment*, 29(4):1179–1189.
- Simpson, E. and Wadsworth, J. (2017). Introduction to Extreme Value Theory and Constructing Hazard Curves. Technical Report January, Lancaster University.
- Sklar, A. (1959). Fonctions de repartition a n dimensions et leurs marges. *Publ. Inst. Statist. Univ. Paris*, 8:229–231.



- Stephenson, A. (2002). evd: Extreme Value Distributions. *R News*, 2(2).
- Tawn, J. A. (1988). Bivariate extreme value theory: Models and estimation. *Biometrika*, 75(3):397–415.
- Vanem, E., Guo, B., Ross, E., and Jonathan, P. (2020). Comparing different contour methods with response-based methods for extreme ship response analysis. *Marine Structures*, 69(August 2019):102680.
- Velarde, J., Vanem, E., Kramhøft, C., and Sørensen, J. D. (2019). Probabilistic analysis of offshore wind turbines under extreme resonant response: Application of environmental contour method. *Applied Ocean Research*, 93:101947.
- Wadsworth, J. L. and Tawn, J. A. (2013). A new representation for multivariate tail probabilities. *Bernoulli*, 19(5 B):2689–2714.
- Wadsworth, J. L., Tawn, J. A., Davison, A. C., and Elton, D. M. (2017). Modelling across extremal dependence classes. *Journal of the Royal Statistical Society. Series B: Statistical Methodology*, 79(1):149–175.

# Supplementary Material

## On the Estimation of Bivariate Return Curves for Extreme Values

C. J. R. Murphy-Barltrop<sup>1\*</sup>, J. L. Wadsworth<sup>2</sup> and E. F. Eastoe<sup>2</sup>

<sup>1</sup>STOR-i Centre for Doctoral Training, Lancaster University LA1 4YR, United Kingdom

<sup>2</sup>Department of Mathematics and Statistics, Lancaster University LA1 4YR, United Kingdom

\*Correspondence to: barltroc@lancaster.ac.uk

May 23, 2022

### Abstract

In the multivariate setting, defining extremal risk measures is important in many contexts, such as finance, environmental planning and structural engineering. In this paper, we review the literature on extremal bivariate return curves, a risk measure that is the natural bivariate extension to a return level, and propose new estimation methods based on multivariate extreme value models that can account for both asymptotic dependence and asymptotic independence. We identify gaps in the existing literature and propose novel tools for testing and validating return curves and comparing estimates from a range of multivariate models. These tools are then used to compare a selection of models through simulation and case studies. We conclude with a discussion and list some of the challenges.

*Keywords:* Risk Measure, Extremes, Dependence Modelling

# 1 Gradients and Lines

Examples of positive gradients and corresponding lines are illustrated in Figure 1 for both copula examples discussed in Section 4.1 of the article. The black lines intersecting the origin correspond to the set of positive gradients  $\mathcal{G}$ . From Figure 1, one can observe that each line (gradient) intersects both the estimated and true return curves exactly once; this follows from the definition of a return curve. In this manner, each gradient and corresponding line represents a common feature of both curves.

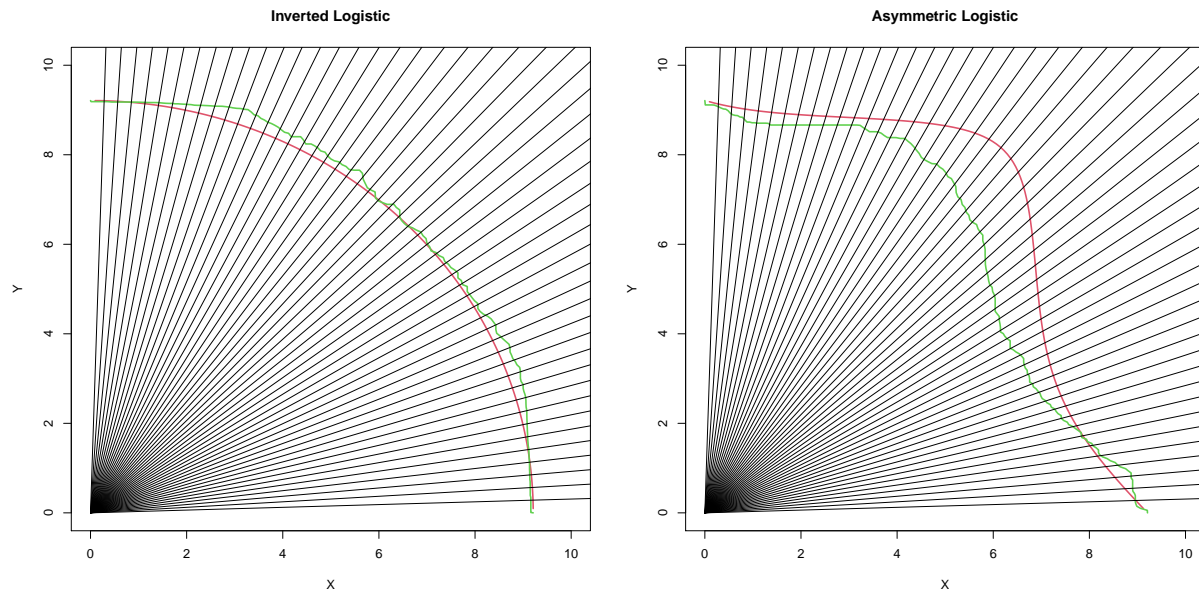


Figure 1: Resulting lines from a set of positive gradients for both copula examples. True and estimated curves given in red and green, respectively.

## 2 Diagnostic Example

In Figure 2, we illustrate the diagnostic tool at different probabilities. The sample size is fixed at  $n = 10^4$  and four probabilities are considered ( $p \in \{10^{-2}, 10^{-3}, 10^{-4}, 10^{-5}\}$ ).

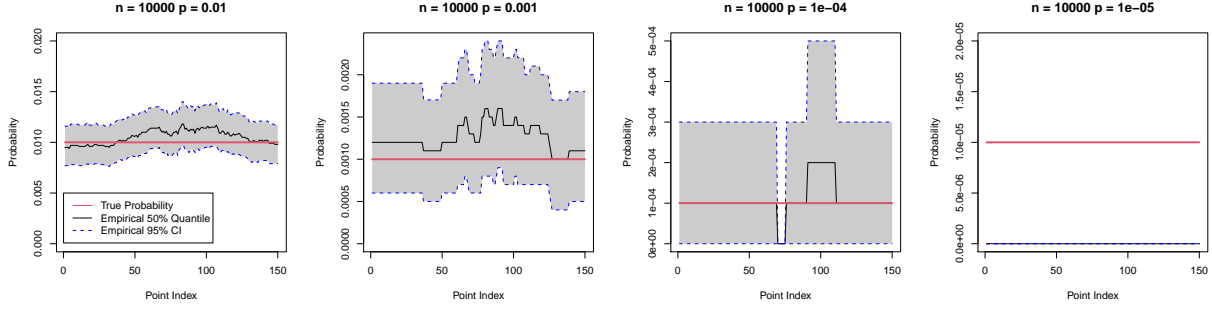


Figure 2: Diagnostic tool for four  $p$  values with logistic copula sample and  $n = 10000$ . Red, black, and dotted blue lines represent true values, estimated medians, and estimated 95% confidence intervals, respectively, for each probability and index  $j$ .

### 3 Summary Statistic

An example of the plot corresponding to the summary statistic is illustrated in the left panel of Figure 3 for a standard bivariate normal copula with  $\rho = 0.6$ , along with the median curve estimates from each model in the right panel. The closer this area is to zero, the closer the norm values are to the truth and hence the nearer the median curve estimates are to the true curve. Moreover, an area of zero corresponds to an unbiased curve estimate since this implies there is no difference between the estimated and true curves (at gradients in  $\mathcal{G}$ ). One can observe the median curve estimate attained using the ? framework appears to perform poorly for this particular example.

### 4 Illustration of procedure for estimating coverage

The left panel Figure 4 illustrates the five gradients used to evaluate coverage. We label these gradients 1-5, clockwise from the  $y$ -axis. Gradient 3 is close in value to one, resulting in a line similar in appearance to  $y = x$ . Gradients 1 and 2 are the multiplicative inverses of gradients 4 and 5, respectively, and hence they can, in a sense, be considered symmetric.

For each simulated sample and gradient  $g$ , a confidence region is obtained for estimated coordinates on the line  $y = gx$ . One can record whether the true point at this gradient

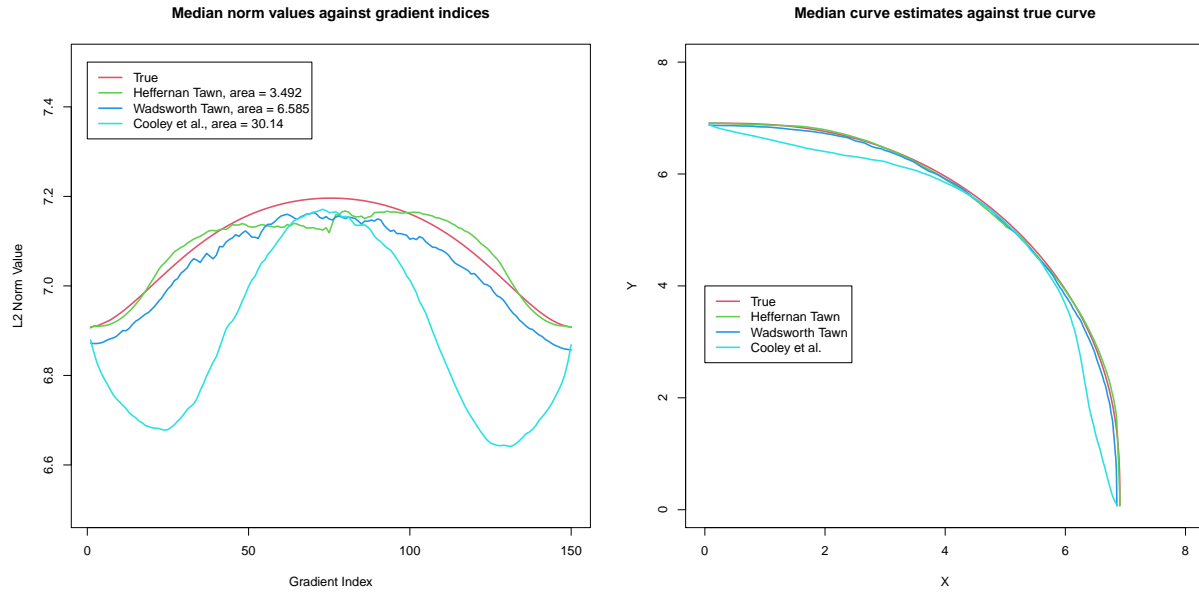


Figure 3: Left: median  $L2$  norm estimates obtained using 250 simulated samples from a standard bivariate normal copula with  $\rho = 0.6$  and true norm values against gradient indices. Summary statistics given in plot legend. Right: median curve estimates from each model against true curve for the same example. True values given in red while the estimated values from the  $?$ ,  $?$  and  $?$  models are given in green, dark blue and light blue, respectively.

lies within the estimated region; for an unbiased curve estimate, this would be expected most of the time. An example confidence region is illustrated in the right panel of Figure 4; we note that the true point (pink) lies within the region. Repeating this procedure over the 500 simulated samples, the proportion of times the true points lie within the estimated confidence regions can be computed, giving an estimated measure of coverage at each of the gradients 1-5.

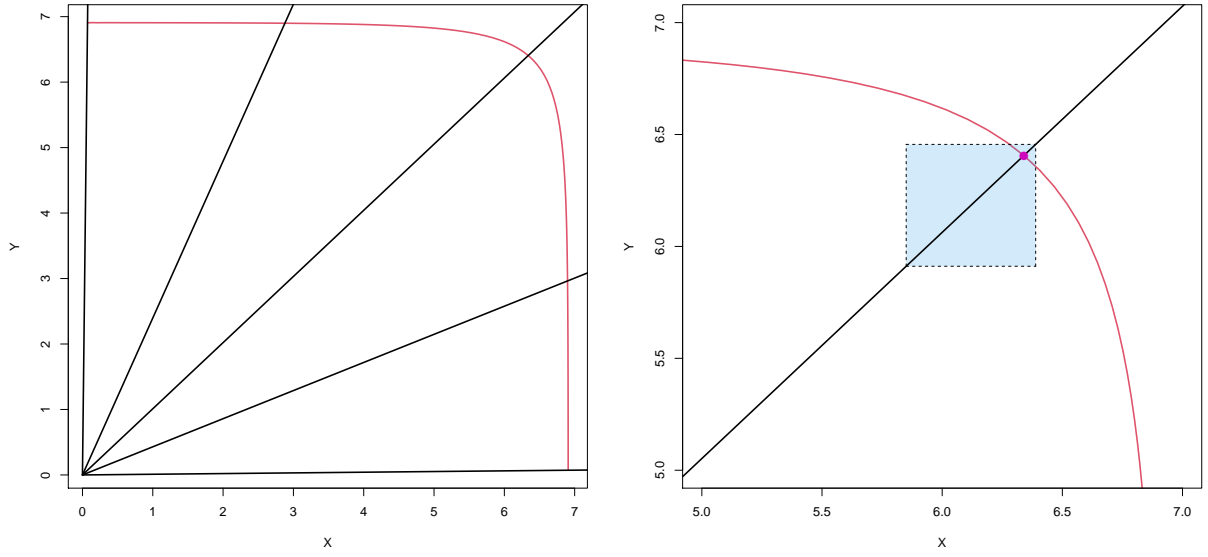


Figure 4: Left: Lines defined by the equation  $y = gx$ , corresponding to the gradients considered for evaluating coverage. Right: Confidence region computed for one sample at the third gradient. The intersection between the blue region and black lines represents the 95% confidence region for norm values. True return curve (red) in both plots obtained from the logistic copula with  $r = 0.5$  and  $p = 10^{-3}$ .

## 5 Additional coverage results

Table 1: Coverage values for  $p = 10^{-4}$ . ‘HT’ and ‘WT’ correspond to the ? and ? models, respectively.

Copula	Probability	$p = 10^{-4}$									
	Model	HT					WT				
BEV Logistic	Gradient	1	2	3	4	5	1	2	3	4	5
	Coverage	0.01	0.97	0.688	*	*	0.844	0.554	0.846	*	*
BEV Asymmetric Logistic	Gradient	1	2	3	4	5	1	2	3	4	5
	Coverage	0.592	0.936	0.496	0.846	0.954	0.902	0	0.008	0.718	0.948
Bivariate Normal 1	Gradient	1	2	3	4	5	1	2	3	4	5
	Coverage	0.474	0.946	0.964	*	*	0.868	0.936	0.906	*	*
Bivariate Normal 2	Gradient	1	2	3	4	5	1	2	3	4	5
	Coverage	0.942	0.928	0.936	*	*	0.936	0.938	0.934	*	*
Inverted BEV Logistic	Gradient	1	2	3	4	5	1	2	3	4	5
	Coverage	0.85	0.928	0.944	*	*	0.86	0.946	0.946	*	*
Inverted BEV Asymmetric Logistic	Gradient	1	2	3	4	5	1	2	3	4	5
	Coverage	0.938	0.928	0.952	0.954	0.902	0.936	0.936	0.954	0.946	0.916
Bivariate T 1	Gradient	1	2	3	4	5	1	2	3	4	5
	Coverage	0.481	0.933	0.419	*	*	0.92	0.672	0.834	*	*
Bivariate T 2	Gradient	1	2	3	4	5	1	2	3	4	5
	Coverage	0.765	0.756	0.854	*	*	0.938	0.554	0.176	*	*
Frank	Gradient	1	2	3	4	5	1	2	3	4	5
	Coverage	0.902	0.816	0	*	*	0.92	0.024	0.01	*	*